Face-dependent Auger neutralization and ground-state energy shift for He in front of Al surfaces

S. Wethekam,[1,*] Diego Valdés,[2] R. C. Monreal,[2] and H. Winter[1]
[1]*Institut für Physik, Humboldt-Universität zu Berlin, Brook-Taylor-Strasse 6, D-12489 Berlin, Germany*
[2]*Departamento de Física Teórica de la Materia Condendada C-V, Universidad Autónoma de Madrid, E-28049 Madrid, Spain*
(Received 20 May 2008; revised manuscript received 14 July 2008; published 20 August 2008)

He atoms and ions with keV energies are scattered under grazing angles of incidence from Al(111), Al(100), and Al(110) surfaces. Fractions of surviving ions and normal energy gains of He^+ ions prior to neutralization, derived from shifts of angular distributions for incident atoms and ions, are compared to results from three-dimensional Monte Carlo simulations based on theoretically calculated Auger neutralization rates and He ground-state energy shifts. From the good agreement of experimental data with simulations, we conclude a detailed microscopic understanding for a model system of ion-surface interactions. Our work provides further evidence for the recently reported surface Miller index dependence for the neutralization of He^+ ions at metal surfaces. The study is extended to the face dependence of the He ground-state energy shift.

DOI: 10.1103/PhysRevB.78.075423 PACS number(s): 79.20.Rf, 79.60.Bm, 61.85.+p

I. INTRODUCTION

A profound understanding of electronic interactions of atoms and ions with solid surfaces is important for a variety of applications as, e.g., surface analytical tools, particle detection, plasma wall interactions, or catalysis. Therefore, a substantial body of work is devoted to the relevant microscopic mechanisms.[1–5] In this respect, the preparation and analysis of model systems where single processes can be studied under well-defined conditions is favorable. Besides resonant tunneling, Auger neutralization (AN) is the second fundamental electron transfer process for ion-surface interactions.[4,6,7] AN is a two-electron process where one electron from the surface is transferred to a bound state (often the ground state) of the atom while the energy is conserved by creation of surface excitations (electron-hole pair or plasmon). Being a two-electron process, AN is generally less efficient than resonant charge transfer and can be best studied for atomic states nondegenerate with occupied electronic states of the surface, a condition met for most noble gas atom-surface combinations. Due to the simple overall electronic structure, He-Al is often referred to as a *model system* for studies on AN.[3,4,7–23] An energy diagram that illustrates the interaction of He atoms with an Al surface is given in Fig. 1. Atomic units (a.u.) are used throughout unless otherwise stated.

Since the pioneering work of Hagstrum,[6] a fair number of experimental and theoretical studies have been devoted to the neutralization of He^+ ions in front of metal surfaces.[2–4,7–18,24] Based on concepts of the classical image potential,[25] He^+ was assumed to be neutralized at distances of about 7 a.u. from the surface, which required AN rates orders of magnitude larger than theoretical predictions. This long-standing discrepancy of experimental and theoretical AN rates was addressed by Merino *et al.*,[11] More *et al.*,[13] and van Someren *et al.*[14] who pointed out that the He ground-state level shift might be substantially reduced compared to the classical behavior for distances of some a.u. in front of the surface. Sophisticated theoretical calculations of the ground-state energy shift showed reduced values or even negative shifts close to the surface as a result of chemical interactions with the surface.[11,13,15] Pronounced deviations of the level shift from the classical behavior were also calculated for the ground state of H (Ref. 26) and for excited states of He in front of an Al surface,[27] and are also predicted for other systems.[28]

Clear-cut experimental evidence that He^+ ions are indeed neutralized close to the surface in accord with the theoretical predictions was provided by the finding that small fractions of He^+ ions grazingly scattered from a metal surface survived the whole scattering event in their initial charge state.[29–32] The surviving ion fractions would have been negligibly small for AN rates derived from experiments using the concept of classical image charges. The picture was completed by measurements of shifts of the high-energy tails of Auger-electron distributions,[16] and shifts of angular distributions for incident neutrals and ions for different energies (different distances of neutralization),[19,22] an experiment proposed by

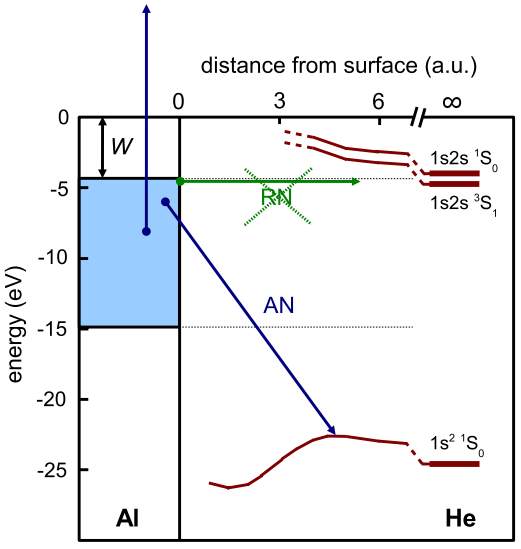

FIG. 1. (Color online) Energy diagram for interaction of He with Al surface. *W*: work function; blue shaded area: occupied states of conduction band of Al; brown curves: energy levels of He as function of distance from the surface for states indicated. Green arrow: resonant neutralization (RN); blue arrows: AN.

More *et al.*[13] that directly measured reduced (and even negative) He ground-state energy shifts close to the surface. A similar downward shift was also found for the ground state of Ar in front of a KCl(001) surface.[33]

Of particular interest are works that compare the neutralization of He^+ ions at different faces of the same metal[32,34,35] where pronounced variations of the surviving ion fractions are observed. These are in accord with the position of the jellium edge as reference for the face-dependent neutralization rates.[32] The studies demonstrate that so-called matrix effects have to be considered in the analysis of low-energy ion scattering (LEIS) (Ref. 36) data for studies on the composition of solid surfaces.[35] Compared to the shift of the reference position for the AN rates (jellium edge) for different faces, the reference positions for the ground-state level shift for the classical region at large (≥ 7 a.u.) distances (image plane) are expected to show smaller shifts.[37,38] However, experimental studies on surface Miller index dependencies of the ground-state energy shift have not been reported so far.

In this work, we present experimental data on the neutralization and the ground-state energy shift for He in front of Al(111), Al(100), and Al(110) surfaces, and compare them with three-dimensional (3D) Monte Carlo simulations based on recent theoretical AN rates and level shifts. Whereas the surviving ion fractions show similar matrix effects as reported for Ag (Refs. 32 and 34) and Cu (Ref. 35) surfaces, the normal energy gains of ions prior to neutralization can be understood using ground-state energy shifts that comprise smaller, although non-negligible, face dependencies. We also show that a quantitative analysis of ion fractions requires the use of AN rates that, even for a given face, depend on the lateral position within the unit cell. The overall agreement of experimental data and theoretical predictions is good for both surviving ion fractions and energy gains without adjustable parameters, which demonstrates that a rather detailed microscopic understanding for this model system of ion-surface interactions has been achieved. This is important to approach with confidence the study of more complex problems such as those involving transition-metal surfaces, surface states,[39] spin-polarized projectiles,[16,40] or the regime of intermediate incident energies where additional charge-transfer processes come into play.[41]

II. EXPERIMENT

In our experiments, we have scattered He^0 atoms and He^+ ions with energies E_0 of some keV under grazing angles of incidence Φ_{in} of typically 1° along high-index ("random") directions from atomically clean and flat Al(111), Al(110), and Al(100) surfaces. The targets were prepared by cycles of grazing sputtering with 25 keV Ar^+ ions and subsequent annealing at 430 °C for about 10 min. During sputtering the target was rotated in order to avoid the formation of patterns on the surface.[42] After dispersion with respect to charge in an electric field, scattered projectiles were detected using a position-sensitive microchannel plate detector. A simple sketch of the experimental setup is shown in the inset of Fig. 2.

For grazing incidence, scattering proceeds in the surface channeling regime[3,43] where the projectiles are steered well above the topmost layer of the surface, and the motions parallel and normal to the surface are widely decoupled. The parallel motion takes place with nearly constant velocity such that the energy can be decomposed into a parallel and a normal component: $E_0 = E_\parallel + E_\perp$, with $E_\parallel = E_0 \cos^2 \Phi_{in}$. The effective impact energy on the surface is given by the normal component of the incident energy $E_\perp^{in} = E_0 \sin^2 \Phi_{in}$, which is of the order of eV for keV projectiles and $\Phi_{in} \sim 1°$.

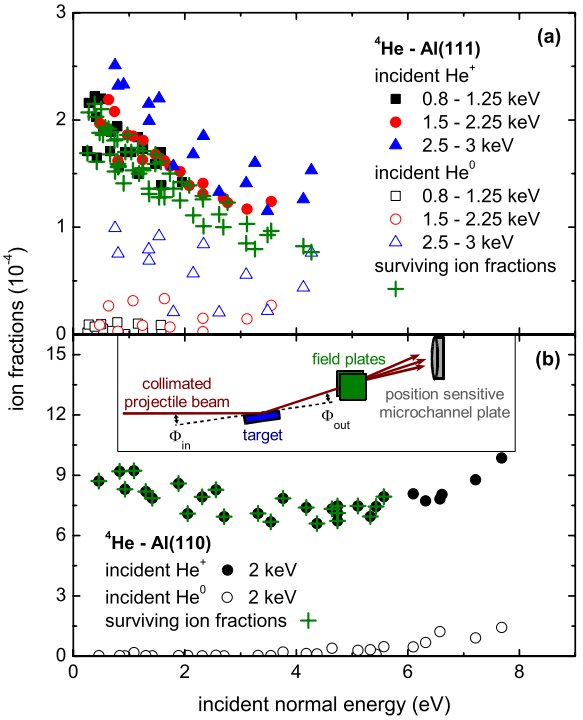

FIG. 2. (Color online) Ion fractions for scattering of He^+ ions (full symbols) and He^0 atoms (open symbols) with energies indicated from Al(111) (panel a) and Al(110) (panel b) as function of incident normal energy. Green plus signs: Surviving ion fractions as used in the analysis below. In the case of He^0 atoms scattered from Al(110), the fractions represent experimental upper limits. The inset shows simple sketch of experiment. For details see text.

A. Experiment techniques

He^+ ions are produced from He gas in an electron cyclotron resonance (ECR) ion source (Pantechnik S.A., Bayeux, France). After acceleration and focusing by an electric lens, projectiles are analyzed with respect to their charge-to-mass ratio in a 90° magnet. Before entering the ultrahigh-vacuum (UHV) chamber, He^+ ions can be neutralized by resonant charge transfer in a gas target operated with He and remaining charged particles are removed by deflection in an electric field. The entrance to the UHV chamber consists of differential pumping stages with turbomolecular pumps separated by three slit systems with horizontal and vertical slits having openings of 0.1–0.2 mm. With a separation of 73 cm, the first and the last slits define the incoming beam to a divergence of less than 0.03°. In order to ensure a negligible bending of ion beams caused by the earth magnetic field, the whole UHV chamber is shielded with μ metal, which results in a reduc-

tion in the magnetic flux of about 95%. 23 cm behind the last pair of slits, projectiles impact the target surface mounted on a precision manipulator that allows for 3D translation, rotation around the axis, and tilting. The base pressure in the target chamber of some 10^{-11} mbar, maintained by turbomolecular and a Ti sublimation pump, ensures that freshly prepared surfaces remain clean for several hours.

Behind the target, scattered projectiles can be analyzed with respect to charge in electric-field plates with an acceptance of $\pm 0.25°$ for the azimuthal angle and no relevant constraint for the polar angle. Polar angular distributions for several charge states can be measured simultaneously with the position-sensitive microchannel plate detector (Roentdek Handels GmbH, Kelkheim-Ruppertshain, Germany) that covers a solid angle of about $4° \times 4°$. The detector is mounted 66 cm behind the target and has an angular resolution of about 0.01°. Electric stray fields of the detector, which might affect trajectories of charged projectiles, are shielded by a surrounding box with a highly transparent grid. As beams with intensities different by several orders of magnitude are compared, special care has to be taken to control and avoid global (time constant ~ 1 μs) and local (time constant $\ll 1$ μs) dead-time effects of the detector. In the so-called histogram mode of the system, typical angular distributions can be measured with intensities of up to 10^4 counts per second with dead-time effects smaller than 5%. Beams with intensities that differ by more than three orders of magnitude are measured separately (one beam being blocked for a defined time) due to a background of the detector of about 10^{-3}. Care was taken to ensure stable beams and all measurements were repeated several times so that beam fluctuations are controlled via the scatter of the data. Saturation effects and background events due to diffuse scattering in the chamber lead to a detection limit for charge fractions of some 10^{-6}.

The detection efficiency of the channel-plate detector varies over its area. For new sets of channel plates, variations of about 5% are observed, which increase with beam exposure. These are especially relevant for low energies of up to a few keV. The local detection efficiency can be monitored and corrected by reference measurements where a beam is wobbled over the active area of the plate, as has been done for the measurements with Al(100) where very accurate charge fractions were needed for the interpretation of isotope effects[21] (see below). All measurements presented in this work were repeated several times using different regions of the channel plate. As our data is derived from comparison of two angular distributions, local variations of detection efficiencies result in a scatter of data around the correct value.

B. Surviving ion fractions

For the study of AN, we have measured fractions of ions that survived the whole scattering event with the surface. Via an integration along the trajectory, these fractions can be closely related to the AN rate [see Eqs. (2) and (4), and below].

In Fig. 2(a) we show ion fractions for scattering of $^4He^+$ ions (full symbols) and $^4He^0$ atoms (open symbols) from Al(111) as function of incident normal energy $E_\perp^{in}$ for different beam energies E_0 indicated. Especially for the two lowest energies, the ion fractions for impact of ions are about an order of magnitude larger than for impact of neutrals, which confirms the former result of an incomplete neutralization along the trajectory and that contributions from reionization of neutralized projectiles are negligible. For energies larger than about 3 keV, reionization processes[41,44,45] set in, as evidenced by the data for incident He^0 atoms. The ion fractions of the order of 10^{-4} reveal that about 99% of the incident ions are neutralized on the incoming part of their trajectory. As reionization processes are restricted to regions very close to the surface (around the turning point of the trajectory), the ion fractions can be corrected for reionization by subtracting the ion fractions for impact of He^0 atoms from the ion fractions for incident He^+ ions. This yields to the so-called surviving ion fractions[46] (green plus signs), which are the basis for the analysis below. For the two lowest energies, these are nearly identical to the ion fractions for incident ions. In passing we note that the additivity of survival and reionization channels, based on their spatial separation, has also been invoked in the interpretation of LEIS experiments.[15,36]

In Fig. 2(b) we show ion fractions for scattering of 2 keV $^4He^+$ ions (full circles) and $^4He^0$ atoms (open circles) from Al(110). The fractions for incident neutrals represent experimental upper limits so that the correction procedure used for Al(111) is not applicable. The surviving ion fractions (green plus signs) are evaluated for normal energies smaller than 6 eV only where reionization is negligible. Although, due to the weaker interaction potential for the more open Al(110) surface, the ions reach distances closer to the surface and should therefore be more efficiently neutralized compared to Al(111), the surviving ion fractions for Al(110) are about a factor of five larger than for Al(111). This can only be understood for a neutralization rate for Al(111) that is larger than for Al(110), which is a clear indication for a pronounced surface Miller index dependence[32,34,35] of the neutralization rate. In this respect, our data provide evidence for this effect for a metal with a jelliumlike electronic structure.

Figures 3(a) and 3(b) present ion fractions for $^4He^+$ and $^3He^+$ ions, as well as upper limits for ion fractions for $^4He^0$ and $^3He^0$ atoms as function of incident normal energy scattered from Al(100) with beam energies indicated. Here, reionization can be neglected and the surviving ion fractions (green plus signs) do not need to be corrected. The surviving ion fractions for $^4He^+$ and $^3He^+$ differ by about a factor of three. This "isotope effect" is a result of the reduced time available for the neutralization of $^3He^+$ compared to $^4He^+$ along the same trajectory.[21] For details we refer to Ref. 21 and the discussion below. The ion fractions for $^4He^+$ ions scattered from Al(100) are intermediate between the results for Al(111) and Al(110), which is again consistent with the interpretation in terms of matrix effects.

C. Normal energy gain

Data on the ground-state energy shift is provided by the gain of normal energy of incident ions prior to neutralization determined from shifts of angular distributions for incident

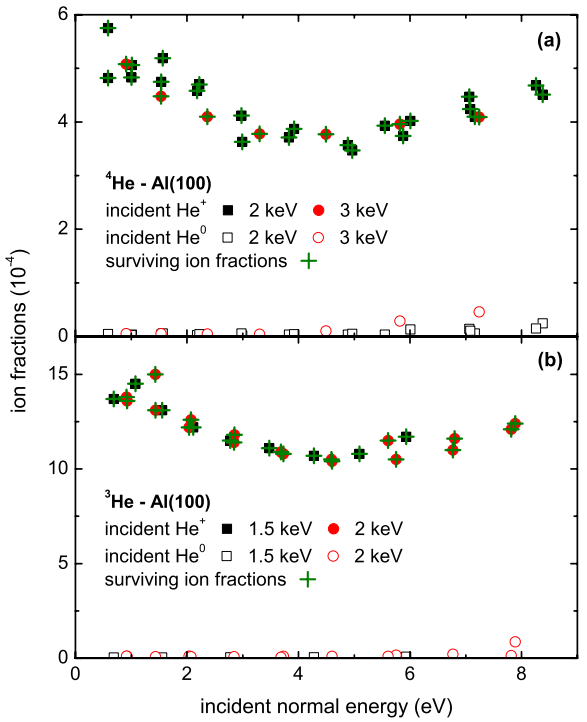

FIG. 3. (Color online) Ion fractions for scattering of $^4He^+$ ions (full symbols, panel a), $^4He^0$ atoms (open symbols, panel a), $^3He^+$ ions (full symbols, panel b), and $^3He^0$ atoms (open symbols, panel b) with energies indicated from Al(100) as function of incident normal energy. Green plus signs: Surviving ion fractions as used in the analysis below. In the case of incident He^0 atoms, the ion fractions represent experimental upper limits. For details see text.

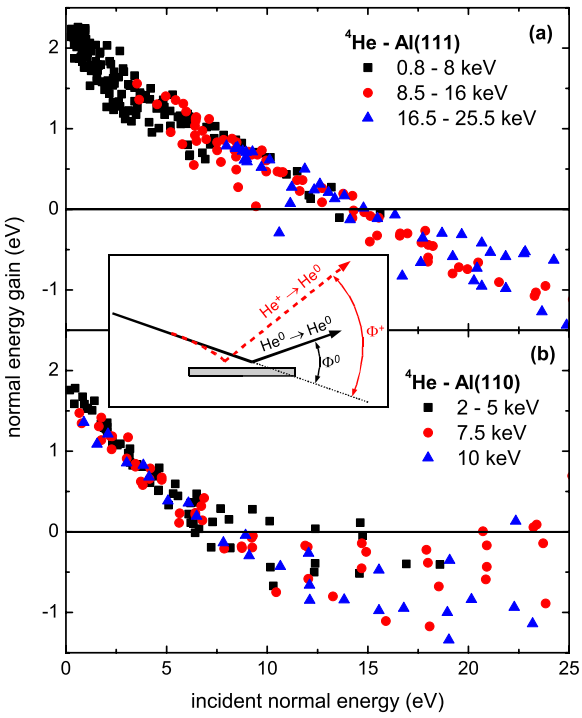

FIG. 4. (Color online) Normal energy gain as function of incident normal energy for scattering of ^4He from Al(111) (panel a) and Al(110) (panel b) for beam energies indicated. The inset shows sketch of trajectories for incident neutrals and ions. For details see text.

ions and neutrals. At the instant of neutralization of an incident ion, its potential energy changes by an amount that is equal to the ground-state energy shift at this position. By variation of the parameters of the incoming beams, the distance of neutralization can be controlled and the ground-state energy shift in front of the surface can be mapped with a tomographic procedure. For details we refer to Refs. 13, 19, and 22, and the analysis performed below.

In Figs. 4(a) and 4(b), we show normal energy gains as function of incident normal energy for ^4He projectiles with beam energies indicated, scattered from Al(111) and Al(110), respectively. The normal energy gain E_{gain} is derived from the peak positions of angular distributions (cf. Fig. 10 and inset of Fig. 4) via

$$E_{gain} = E_{\perp}^{out,+} - E_{\perp}^{in} = E_0[\sin^2(\Phi^+ - \Phi^0/2) - \sin^2(\Phi^0/2)], \quad (1)$$

where $E_{\perp}^{out,+}$ is the outgoing normal energy for neutralized ions with an incident normal energy $E_{\perp}^{in}$. These are calculated from the scattering angles for incident ions Φ^+ and neutrals Φ^0. The grazing angle of incidence is close to $\Phi^0/2$ for He^0 atoms elastically reflected from the surface. As expected for surface channeling with velocities much smaller than the Bohr velocity (1 a.u.),[3,43] the data depend on features of the normal motion only. This shows that dynamic effects can be neglected here.

The normal energy gains show a pronounced dependence on the incident normal energy. For low normal energies, i.e., neutralization further away from the surface, the normal energy gains are about +2 eV, which agrees well with typical shifts of the high-energy cutoffs of Auger-electron distributions for low-energy He^+ impact on metal surfaces.[6,16,24] These can be understood on the basis of classical image charge potential shifts of the ground-state energy. However, for increased normal energies, i.e., neutralization closer to the surface, the normal energy gain is reduced and changes sign. This corresponds to a downward shift of the ground-state energy close to the surface due to short-range chemical interactions.[13,15,16,19,20,22]

Our data on the normal energy gain as function of incident normal energy for ^4He and ^3He projectiles scattered from Al(100) (beam energies indicated) is given in Figs. 5(a) and 5(b), respectively. For ^4He the normal energy gains are intermediate between the results for Al(111) and Al(110), which is consistent with the expected face dependencies. Due to its smaller mass, $^3He^+$ approaches the surface on a shorter time scale than $^4He^+$ for the same incident normal energy, which results in neutralization closer to the surface. Therefore, the crossover of the normal energy gain for ^3He appears at smaller incident normal energies. A more detailed discussion can be found in Sec. IV B. Finally, we mention that the experimental uncertainties for the data presented in this section are estimated to be as large as the scatter of data points.

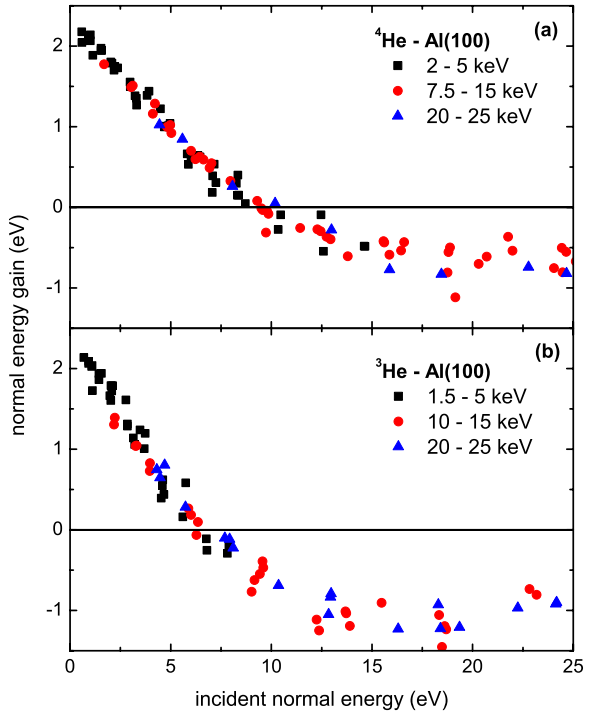

FIG. 5. (Color online) Normal energy gain as function of incident normal energy for scattering of ^{4}He (panel a) and ^{3}He (panel b) from Al(100) for beam energies indicated. For details see text.

III. THEORY MODEL

For comparison with our data, we have performed 3D Monte Carlo simulations based on recent theoretical AN rates $\Gamma_{AN}(\vec{r})$ and ground-state energy shifts[20] $\Delta E_{1s}(\vec{r})$. For each time step in the simulations, the Newton equations of motion for the projectile and the target atoms, as well as the differential equation for the population P^+ of the ionic state,

$$dP^+ = -P^+\Gamma_{AN}(\vec{r})dt, \tag{2}$$

are numerically solved using a fourth-order Runge-Kutta method.[47] After each step, the charge state of the projectile is determined by comparing P^+ to a random number. Close to the surface, we use 25 steps per 1 a.u. distance, which ensures negligible numerical errors, so that the main uncertainties of the simulations result from the interpolation of rates and level shifts between the calculated points. In the simulations, the Al surfaces are represented by clusters consisting of two layers of 7×7 atoms centered below the projectile. For each trajectory, the initial position of a projectile is chosen randomly with respect to a unit cell of the surface. Correlated thermal displacements of target atoms are included within the Debye model at $T=300$ K and Debye temperatures from Ref. 48. For details see Ref. 49. In the simulations, the experimental angular acceptance for the azimuthal direction with respect to the incoming beam of $\pm0.25°$ is included. Although angular distributions are often broader, the limited detection window turns out to be of minor importance (maximum changes of a factor of two for the surviving ion fractions are observed). This is due to the fact that the quantities discussed in this work result from comparisons of two distributions. There are no relevant limitations for the polar detection angle in the experiment. Further input for the simulations is discussed in the following.

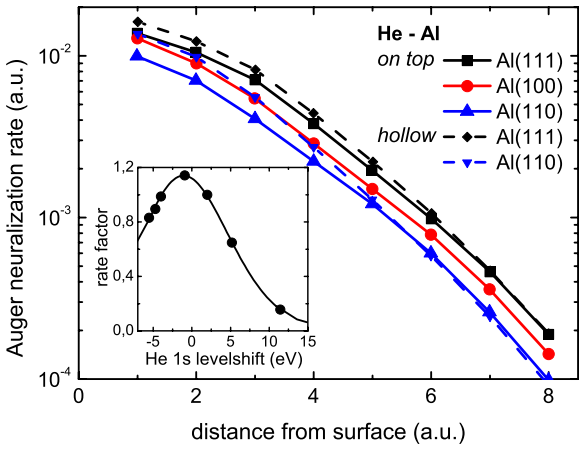

FIG. 6. (Color online) Auger neutralization rates for He^+ in front of Al(111) (black solid curve with squares), Al(100) (red solid curve with dots), and Al(110) (blue solid curve with upward triangles) for the on top as well as Al(111) (black dashed curve with diamonds) and Al(110) (blue dashed curve with downward triangles) for the hollow lateral positions calculated in Ref. 20 using a basis set of atomic orbitals as function of distance from topmost layer of surface. The inset shows rate enhancement factor as function of ground-state energy shift. For details see text.

A. Auger neutralization rates

In Fig. 6 we show AN rates for the neutralization of He^+ ions in front of Al(111) (black solid curve with squares), Al(100) (red solid curve with dots), and Al(110) (blue solid curve with upward triangles) for the on top, as well as Al(111) (black dashed curve with diamonds) and Al(110) (blue dashed curve with downward triangles) for the hollow lateral positions calculated using a basis set of atomic orbitals in Ref. 20. The calculations were performed for a constant ground-state energy shift of +2 eV from which the AN rates for different ground-state energy shifts can be obtained by multiplication with a factor given in the inset of Fig. 6, also calculated in Ref. 20. In accordance with our interpretation of the surviving ion fractions (cf. Sec. II B), the calculated AN rates increase in the sequence Al(110), Al(100), and Al(111). This can be understood by the different spill out of the electron density, i.e., different jellium edges [Al(110): 1.35 a.u.; Al(100): 1.91 a.u.; Al(111): 2.21 a.u.], for the three faces.[20] When plotted as function of distance from the jellium edge, the rates for the different faces nearly coincide for distances to the surface larger than 5–6 a.u.. This means that, at these distances, the values of the rates for the different faces are determined by the position of the jellium edge only. However, at closer distances, Fig. 6 shows that, for a given face, there is also an important dependence of the AN rate on the lateral position of the ion within the unit cell. This dependence is more pronounced for the open (110) face than for the close-packed (111) surface. Then, with respect to AN, Al surfaces do not behave like free-electron ones. In Sec. IV

we will show results of simulations performed using the on-top site and hollow-site AN rates demonstrating the sensitivity of the ion fractions to these quantities.

B. Interaction potential and He ground-state energy shift

For the calculation of trajectories for He^0 atoms, we made use of a Moliere potential with a screening length modified by O'Connor and Biersack (OCB).[50] This choice is different from Refs. 19 and 22 where an interaction potential derived from data for rainbow scattering under axial surface channeling[51] was used. Although being very sensitive to the interaction potential, the rainbow data does not yield enough information for an unequivocal derivation of the potential and, without further input, very different potentials can be constructed from the data.[52] Therefore, in the former ansatz based on a reduced OCB potential and an uncorrugated embedding contribution,[53] which was needed to reproduce the small rainbow angles at low energies, the free parameters were fixed by a calculated potential[54] for very small energies ≤ 0.7 eV. For more details, we refer to Ref. 22.

The OCB potentials without (solid black curve) and including thermal displacements (dashed red curve) of target atoms as well as the "rainbow" (RB) potential (dash-dotted blue curve) for He-Al(111) averaged parallel to the surface are depicted in Fig. 7(b). While the OCB potential shows a continuous increase, the RB potential has a shoulder at 3.7 a.u. in front of the surface that, in the model, results from a repulsive contribution to the potential due to embedding He^0 into the electron gas. However, although consistent with a calculated potential,[54] a shoulder much further away from the surface than the jellium edge at 2.21 a.u. does not appear reasonable. In addition, the shoulder results in very different distances of closest approach for projectiles with normal energies in the range of 1–5 eV. As projectiles that reach distances closer to the surface are more strongly affected by the corrugation of the surface, this would have strong consequences for the width of angular distributions. In Fig. 7(a) we show the full width at half maximum (FWHM) of polar angular distributions for scattering of $^4He^0$ atoms from Al(111) (cf. Fig. 10) as function of grazing angle of incidence (beam energies indicated). The experimental widths (full symbols) show a pronounced dependence on the angle of incidence but do only slightly depend on the beam energy. The data is in perfect agreement with our simulations for the OCB potential (solid curves with open symbols) while the agreement with the potential derived from the rainbow data (dotted curves) is poorer. This is a consequence of the soft slope of the RB potential. In conclusion, we decided for the OCB potential in this work.

The He ground-state energy shift as function of distance from Al(111), calculated for the on-top position in Ref. 20, is plotted in Fig. 8 (green dots). The interpolation used in our simulations is given by the green dash-dotted curve. At large distances $z \geq 7$ a.u., the level shift follows the behavior expected for classical image charge interactions[25] but, close to the surface, the level shifts downward as a result of short-range chemical interactions in accordance with our experimental findings in Sec. II C. At distances $z < 2$ a.u., the level

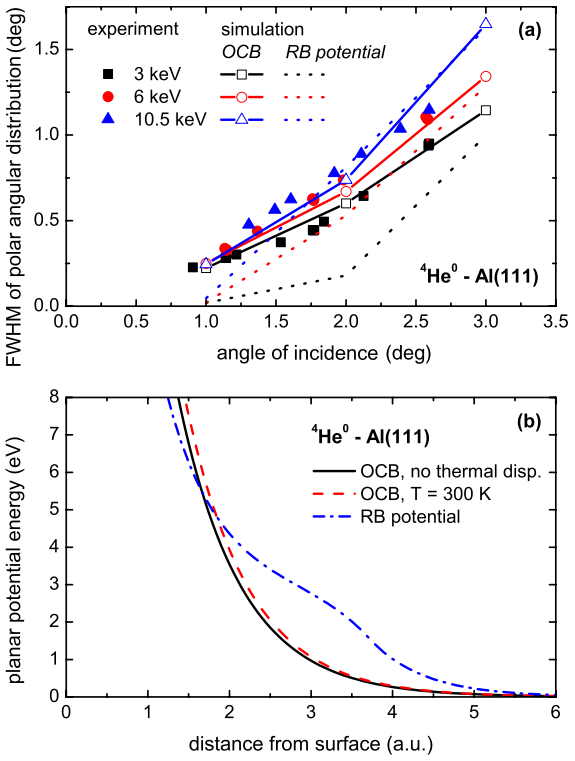

FIG. 7. (Color online) Panel a: FWHM of polar angular distributions as function of angle of incidence for $^4He^0$ atoms scattered from Al(111) with beam energies indicated. Experimental results (full symbols) are compared to simulations using the RB potential from Refs. 19 and 22 (dotted curves), and the OCB potential (Ref. 50) (solid curves with open symbols). Panel b: OCB potentials without (solid black curve) and including thermal displacements (dashed red curve) of target atoms, and RB potential (dash-dotted blue curve) for $^4He^0$-Al(111) averaged parallel to the surface as function of distance from the surface. For details see text.

is promoted by the interaction with the Al core orbitals. In a simple picture this can be understood in terms of spatial limitations for the wave function.[55] We note that this range of interatomic distances is not relevant here. As discussed above, in the present case of small perpendicular energies, the surviving ion fractions relate to the Auger rates at distances larger than about 2 a.u.. The same applies to the normal energy gains from Sec. II C as the peak positions of the angular distributions result from the majority of ions neutralized on the incoming part of the trajectory, and the data for different beam energies coincide while the additional charge-transfer processes are confined to a region very close to the surface and have a strong dependence on energy.

As the ground-state energy shift [green dash-dotted curve in Fig. 8(a)] corresponds to the on-top position, it is evaluated as function of distance to the closest target atom (with slight modifications to ensure continuity) in our simulations. The solid black, dashed red, and dotted blue curves in Fig. 8(a) depict the level shift averaged parallel to Al(111), Al(100), and Al(110), respectively. The energy shifts coincide for large distances, which is the correct behavior due to the small differences of the image plane positions,[37,38] and show the expected relative behavior close to the surface. This

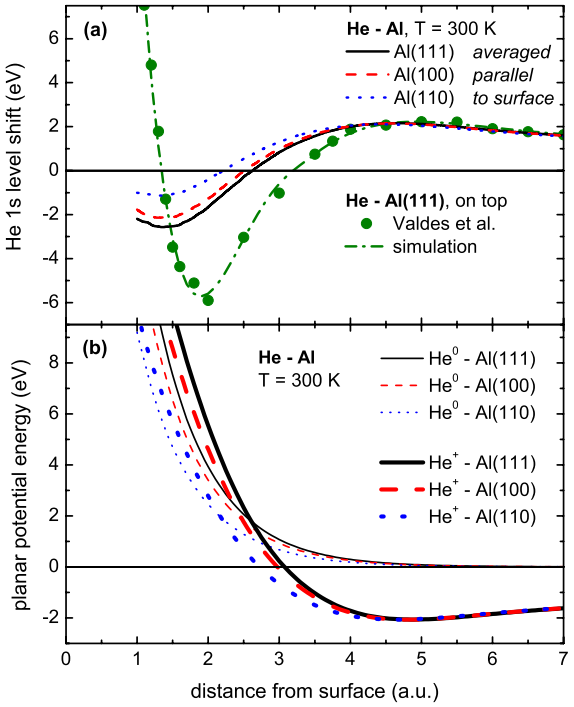

FIG. 8. (Color online) Panel a: He ground-state energy shift as function of distance from Al(111) surface calculated for on-top position in Ref. 20 (green dots) and values used in the simulations (green dash-dotted curve). Black solid, red dashed, and blue dotted curves: level shifts averaged parallel to surface for Al(111), Al(100), and Al(110). Panel b: potential energy averaged parallel to surface as function of distance for He^0 (thin curves) and He^+ (thick curves) in front of Al(111) (black solid curves), Al(100) (red dashed curves), and Al(110) (blue dotted curves). For details see text.

averaged value is the one that has to be related to the energy gain measured in the present experiments. At very grazing angles of incidence and random azimuthal directions, ions spend a long time traveling parallel to the surface and therefore probe many different lateral positions within the unit cell.

The ground-state energy shift,

$$\Delta E_{1s}(\vec{r}) = E_{1s}(\vec{r}) - E_{1s}(\infty) = V_{He^0}(\vec{r}) - V_{He^+}(\vec{r}), \qquad (3)$$

is directly related to the difference in interaction potentials for He^0 atoms $V_{He^0}(\vec{r})$ and He^+ ions $V_{He^+}(\vec{r})$ in front of the surface.[3,4,13,15,19,20,22,25] Therefore, the interaction potential for He^+ ions used in the simulations is constructed from the level shift and the potential for neutrals using Eq. (3). The potentials $V_{He^0}(\vec{r})$ (thin curves) and $V_{He^+}(\vec{r})$ (thick curves) averaged parallel to Al(111) (solid black curves), Al(100) (dashed red curves), and Al(110) (dotted blue curves) are shown in Fig. 8(b). As expected, the potentials are strongest for the most densely packed surface, Al(111), and are weakest for the most open surface, Al(110).

IV. RESULTS AND DISCUSSION

We compare results from our 3D Monte Carlo simulations, based on the theoretical input described in the previous section, to our experimental data. Both the surface Miller index dependence of the surviving ion fractions and normal energy gains are in good accord with our data. The same holds for the isotope effects observed for ^{3}He and ^{4}He scattered from Al(100).

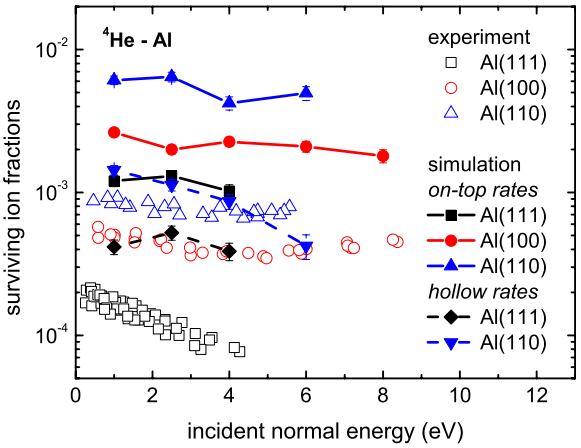

FIG. 9. (Color online) Experimental surviving ion fractions from Figs. 2 and 3 as function of incident normal energy for $^4He^+$ ions scattered from Al(111) (black open squares), Al(100) (red open dots), and Al(110) (blue open upward triangles) compared to simulations using on-top AN rates for Al(111) (solid black curve with full black squares), Al(100) (solid red curve with full dots), and Al(110) (solid blue curve with full upward triangles) as well as AN rates for hollow position for Al(111) (black dashed curve with full diamonds) and Al(110) (blue dashed curve with full downward triangles). Error bars represent statistical uncertainties. For details see text.

A. Surface Miller index dependence

In Fig. 9, our measured surviving ion fractions for $^4He^+$ ions scattered from Al(111) (black open squares), Al(100) (red open dots), and Al(110) (blue open upward triangles) are compared to simulations based on the on-top AN rates [Al(111): black solid curve with full squares, Al(100): red solid curve with full dots, Al(110): blue solid curve with full upward triangles] as well as AN rates for the hollow position [Al(111): black dashed curve with full diamonds, Al(110): blue dashed curve with full downward triangles]. The relative dependence of the ion fractions with crystal face is reproduced by the simulations. However, the on-top rates give ion fractions much larger than those in the experiment while use of the hollow rates yields much better agreement, especially in the case of the open Al(110) surface. This is to be expected because at random directions an ion is, most of the time, above hollow-site positions in the unit cell.

The results of Fig. 9 clearly show the extreme sensitivity of the ion fractions to the values of the AN rate. This can be seen from integration of Eq. (2) along a trajectory of an ion

$$P^+ = \exp\left(-\int_{\text{tra.}} \Gamma_{AN} dt\right), \qquad (4)$$

which yields an exponential dependence of the surviving ion fractions on the AN rate. Then, an increase in the rates by

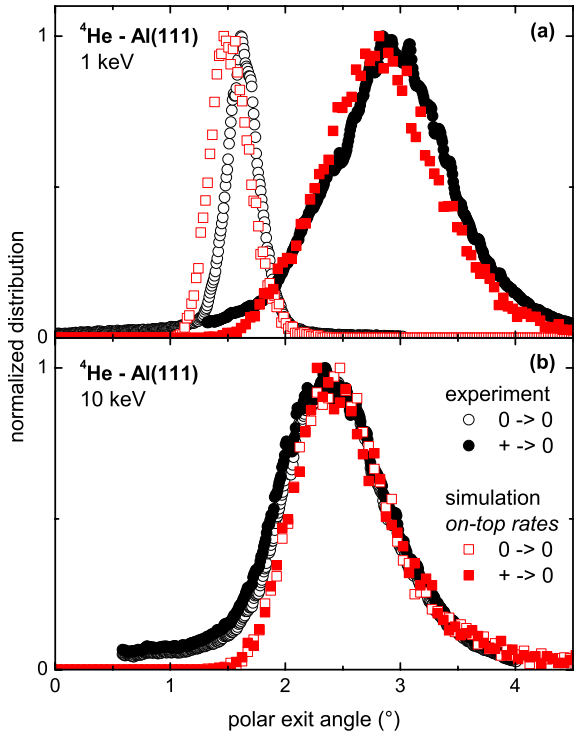

FIG. 10. (Color online) Polar angular distributions for scattering of 1 (panel a) and 10 keV (panel b) $^4He^+$ ions (full symbols) and $^4He^0$ atoms (open symbols) from Al(111). Black dots (red squares) show experimental data (simulation for on-top rates). For details see text.

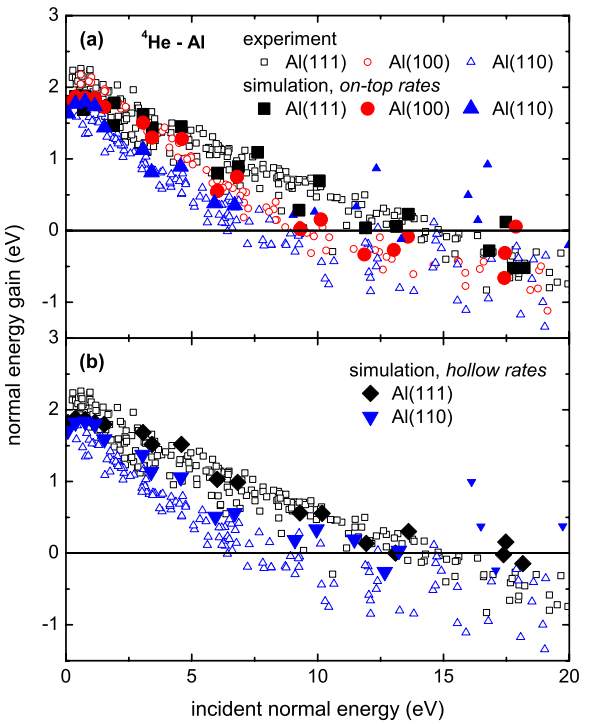

FIG. 11. (Color online) Experimental normal energy gains from Figs. 4 and 5 as function of incident normal energy for ^{4}He scattered from Al(111) (black open squares), Al(100) (red open dots), and Al(110) (blue open squares) compared to simulations using on-top AN rates (panel a) for Al(111) (black full squares), Al(100) (red full dots), and Al(110) (blue full upward triangles) as well as AN rates for the hollow position (panel b) for Al(111) (black full diamonds) and Al(110) (blue full downward triangles). For sake of clarity, results of simulations for Al(110) at large normal energies (neutralization close to surface), where our model for the ground-state energy shift breaks down, are shown with smaller symbols. For details see text.

30% reduces the ion fractions by factors of about five to ten. Therefore, the fact that the agreement between theory and experiment is systematically improved by using the hollow position rates shows the importance of a proper description of the face dependence of the AN rate beyond the simple jellium edge concept. A better treatment of the neutralization process along the trajectory, using position-sensitive AN rates, may give a better agreement between theory and experiment. We should also mention that the intrinsic uncertainty of density-functional theory calculations of AN rates due to inevitable approximations, such as neglect of quantum indistinguishability of the electrons involved in the process, are estimated to about 20% (Refs. 7, 9, and 56), and the deviations of experiment and simulation are on this level.

Experimental (black dots) and simulated (red squares, on-top rates) polar angular distributions for scattering of 1 (panel a) and 10 keV (panel b) $^4He^+$ ions (full symbols) and $^4He^0$ atoms (open symbols) from Al(111) are given in Fig. 10. The distributions in panel a for incident ions, which correspond to an incident normal energy of about 0.8 eV, are clearly shifted toward larger outgoing angles compared to the distributions for incident atoms. Via Eq. (1) this is related to a positive normal energy gain due to neutralization at large distances from the surface where the ground-state energy shift is positive. Panel b shows data for a larger incident normal energy of about 17 eV where shifts of the distributions for incident ions and neutrals are absent. The normal energy gain is close to zero (cf. also Fig. 4), which means neutralization at about 3 a.u. in front of the surface where the ground-state energy shift changes sign (cf. Fig. 8). The overall agreement of measured and simulated distributions including the tails is good, which shows that our simulations catch the main ingredients of the physics involved. In addition it can be concluded that the density of surface defects is negligibly small.[57]

Measured (open symbols) and simulated (full symbols) normal energy gains as function of incident normal energy for scattering of $^4He^+$ ions from Al(111) (black squares), Al(100) (red dots), and Al(110) (blue upward triangles) for the on-top rates are compared in Fig. 11(a). Figure 11(b) shows a comparison of the experimental normal energy gains and simulations based on the hollow-site rates for Al(111) (black diamonds) and Al(110) (blue downward triangles). The experimental data is the same as in Figs. 4 and 5. As both experimental data and simulations scale well with the normal energy, the beam energies are not labeled in Fig. 11 for sake of clarity. Simulations have been performed for 1–25 keV atoms and ions. The angular distributions from the simulations have been analyzed with respect to shifts by the same procedure as applied to the experimental distributions.

The differences between the normal energy gain for different faces can be understood from a ground-state energy

shift with a weaker face dependence than the AN rate. As the AN rate for Al(111) is larger than for Al(110) (see Secs. II B and III A), the incident normal energy that results in the same distance of neutralization is larger for Al(111) than for Al(110). Therefore, for Al(111), the downward shift of the level is seen at larger incident normal energies. Measured and simulated normal energy gains agree on a quantitative level, which shows that the calculated level shifts are accurate. Only the simulations for Al(110) for large normal energies after the crossover of the normal energy gain (see smaller symbols), where also the relative effects get very small, show small deviations from the experimental data. This is a result of our implementation of the ground-state energy shift for the three faces, based on the on-top level shift for Al(111) evaluated as function to the closest target atom (cf. Sec. III B). This ansatz will be least valid for Al(110) as it represents the most open surface with the smallest AN rate and therefore closest distance of neutralization for incident ions. However, in the region before the zero crossing where the effects of the downward shift are most pronounced, the agreement is very good. Also, the fact that we never measure energy gains smaller than −1 eV is consistent with our interpretation of the energy gain as average of level shifts parallel to the surface [plotted in Fig. 8(a)]. We can thus conclude that neutralization of He^+ ions takes place at distances between 2 and 4 a.u. for perpendicular energies smaller than 20 eV.

B. Isotope effect

Different isotopes of the same element scattered with the same incident angle and energy from a surface follow the same trajectories but on different time scales (if the energy transfer to the surface is negligible, which holds for the grazing geometry[3,43]). The isotope effect for the surviving ion fractions has been used to demonstrate the existence of a well-defined neutralization rate such that transient populations of excited states during the neutralization process can be neglected,[21] in accord with the results of Ref. 13. For details we refer to Ref. 21.

The isotope effect for the surviving ion fractions (cf. Fig. 3) can be understood on the basis of Eq. (4) when the integration over time is substituted by an integration of a line element ds along the trajectory divided by the velocity expressed in terms of the kinetic energy $E_{\mathrm{kin}}(\vec{r})$ and the mass M of the projectile. This yields a scaled expression, independent of isotope mass:

$$\frac{\ln(P^+)}{\sqrt{M}} = -\int_{\mathrm{tra.}} \frac{\Gamma_{\mathrm{AN}}(\vec{r})}{\sqrt{2E_{\mathrm{kin}}(\vec{r})}}\mathrm{d}s. \tag{5}$$

A pronounced isotope effect is also seen for the normal energy gain. As $^3He^+$ ions approach the surface faster than $^4He^+$ ions with the same normal energy, they are neutralized closer to the surface where the ground-state energy is shifted more downward; an effect clearly present in the data in Fig. 5. The relevant quantity that determines the distance of neutralization is the normal velocity. As a result of slight modifications of the normal velocity, different for the two isotopes, due to the interaction potential at the surface, this scaling is not exact as in the case of the surviving ion fractions.

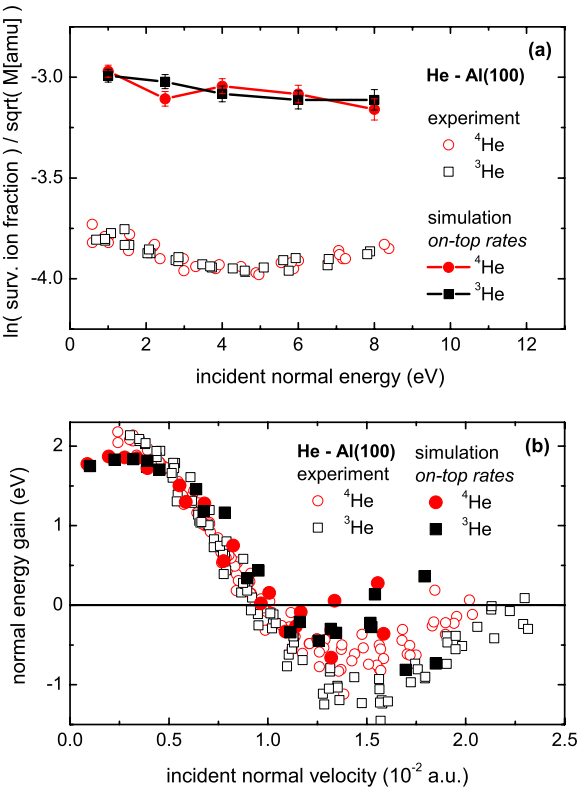

FIG. 12. (Color online) Panel a: experimental surviving ion fractions P^+ from Fig. 3 scaled for isotope effect [cf. Eq. (5)], $\ln(P^+)/\sqrt{M[\mathrm{amu}]}$, for $^4He^+$ (red open dots) and $^3He^+$ (black open squares) scattered from Al(100) compared to simulations for $^4He^+$ (red curve with full dots) and $^3He^+$ (black curve with full squares) as function of incident normal energy. Error bars represent statistical uncertainties. Panel b: experimental normal energy gains for $^4He^+$ (red open dots) and $^3He^+$ (black open squares) scattered from Al(100) compared to simulations for $^4He^+$ (red full dots) and $^3He^+$ (black full squares) as function of incident normal velocity. Simulations were performed for on-top AN rates. For details see text.

In Fig. 12(a) we show the experimental ion fractions of Fig. 3 as function of incident normal energy, scaled with respect to the isotope effect according to Eq. (5), for $^4He^+$ (red open dots) and $^3He^+$ (black open squares) scattered from Al(100). These are compared to simulations for $^4He^+$ (red curve with full dots) and $^3He^+$ (black curve with full squares) based on the on-top rates. For both experimental data and simulations, the scaling works well and demonstrates that the conclusions in Ref. 21 are not modified by unexpected complex trajectory effects or the restricted detection window in the experiment. In Fig. 12(b) experimental (open symbols) and simulated (full symbols) normal energy gains for $^4He^+$ ions (red dots) and $^3He^+$ (black squares) are plotted as function of the incident normal velocity. The agreement of data and simulations is good, and shows a scaling with the incident normal velocity.

V. SUMMARY AND CONCLUSIONS

We have presented experimental results and simulations based on theoretical AN rates and He ground-state energy

shifts for the surviving ion fractions, as well as normal energy gains for grazing scattering of different isotopes of He with keV energies from three faces of Al, namely Al(111), Al(100), and Al(110). In accord with recent theoretical predictions[20,32] and recent experimental results for Ag (Refs. 32, 34, and 58) and Cu surfaces,[35] we present experimental evidence for pronounced Miller index dependencies (a special case of matrix effects in LEIS) for the neutralization of He in front of a jellium metal. Our findings are in good accord with our simulations, which show that the effects are related to different reference positions for the AN rates for the three faces. The jellium edge serves as a good reference in this respect although accurate lateral position dependent Auger neutralization rates might be needed for a more detailed quantitative analysis of experiments.[59]

In a second set of experiments, we present the results on the surface Miller index dependence of the He ground-state energy shift by measuring the normal energy gain of ions prior to neutralization via shifts of angular distributions of incident ions and neutrals.[13,19] The data shows pronounced face dependencies and is in quantitative accord with simulations based on the on-top He ground-state level shift calculated for He-Al(111) evaluated as function of distance to the closest target atoms. For the different faces, this yields similar level shifts at large distances, in accord with theoretical predictions,[37,38] and a pronounced dependence on the surface-atom density close to the surface due to the binary character of electron promotion. The results of our full simulations can be envisioned in terms of an averaging of level shifts and AN rates parallel to the surface. This allows us to conclude that He^+ ions incident on Al with perpendicular energies smaller than 20 eV are neutralized by Auger processes at distances between 2 and 4 a.u. in front of the surface.

Also data on the isotope effect of the surviving ion fractions, and the normal energy gains for ^{3}He and ^{4}He projectiles are in good accord with our simulations. Our studies on the isotope scaling properties provide further evidence for the interpretation in Ref. 21 in terms of the existence of a well-defined neutralization rate and minor contributions of excited states in the neutralization process.[13]

The overall agreement of our simulations, free from adjustable parameters, with the experimental data is good and deviations are on a level of the intrinsic uncertainties of the calculations due to inevitable approximations such as neglect of quantum indistinguishability of the electrons involved.[7,9,56] We therefore conclude that a detailed microscopic understanding for this model system of ion-surface interactions has been achieved. This is important to approach with confidence more complicated problems involving, i.e., transition-metal surfaces and/or problems where additional charge-exchange mechanisms come into play.

Finally, we mention that, despite the extreme sensitivity of the experimental data on the underlying physical quantities, i.e., AN rate and ground-state energy shift, we have not adjusted those to the data. The interplay of level shift and interaction potential, and thus of normal energy gain and surviving ion fractions, would not provide unequivocal conclusions.[22] In addition, we have to stress that the He^0-Al interaction potential was not derived from our theory but represents a reasonable approach only (see Sec. III B). Based on accurate 3D theoretical interaction potentials tested in detail via rainbow scattering along low-indexed directions,[22,51] a more sophisticated comparison of experimental and theoretical AN rates, and He ground-state energy shifts is feasible. Based on the detailed experimental information, we hope that our study triggers in-depth theoretical treatments for this model system of atom-surface interactions.

ACKNOWLEDGMENTS

We thank the DFG (Project No. Wi 1336) for financial support, and G. Adamov, K. Maass, A. Mertens, and A. Schüller for their assistance in the experiments. This work has been funded by the Spanish Ministerio de Educación y Ciencia (Project No. FIS2005-02909).

*Author to whom correspondence should be addressed. stephan.wethekam@physik.hu-berlin.de

[1] J. Los and J. J. C. Geerlings, Phys. Rep. **190**, 133 (1990).
[2] H. Niehus, W. Heiland, and E. Taglauer, Surf. Sci. Rep. **17**, 213 (1993).
[3] H. Winter, Phys. Rep. **367**, 387 (2002).
[4] R. C. Monreal and F. Flores, Adv. Quantum Chem. **45**, 175 (2004).
[5] J. P. Gauyacq, A. G. Borisov, and M. Bauer, Prog. Surf. Sci. **82**, 244 (2007).
[6] H. D. Hagstrum, Phys. Rev. **96**, 336 (1954).
[7] M. A. Cazalilla, N. Lorente, R. D. Muiño, J. P. Gauyacq, D. Teillet-Billy, and P. M. Echenique, Phys. Rev. B **58**, 13991 (1998).
[8] R. Monreal and N. Lorente, Phys. Rev. B **52**, 4760 (1995).
[9] N. Lorente and R. Monreal, Surf. Sci. **370**, 324 (1997).
[10] R. Monreal, Surf. Sci. **388**, 231 (1997).
[11] J. Merino, N. Lorente, W. More, F. Flores, and M. Yu. Gusev, Nucl. Instrum. Methods Phys. Res. B **125**, 250 (1997).
[12] T. Hecht, H. Winter, and A. G. Borisov, Surf. Sci. **406**, L607 (1998).
[13] W. More, J. Merino, R. Monreal, P. Pou, and F. Flores, Phys. Rev. B **58**, 7385 (1998).
[14] B. van Someren, P. A. Zeijlmans van Emmichoven, and A. Niehaus, Phys. Rev. A **61**, 022902 (2000).
[15] N. P. Wang, E. A. Garcia, R. Monreal, F. Flores, E. C. Goldberg, H. H. Brongersma, and P. Bauer, Phys. Rev. A **64**, 012901 (2001).
[16] J. C. Lancaster, F. J. Kontur, G. K. Walters, and F. B. Dunning, Phys. Rev. B **67**, 115413 (2003).
[17] F. A. Gutierrez and H. Jouin, Phys. Rev. A **68**, 012903 (2003).
[18] E. A. Garcia, N. P. Wang, R. C. Monreal, and E. C. Goldberg, Phys. Rev. B **67**, 205426 (2003).
[19] S. Wethekam and H. Winter, Surf. Sci. **596**, L319 (2005).

[20] Diego Valdés, E. C. Goldberg, J. M. Blanco, and R. C. Monreal, Phys. Rev. B **71**, 245417 (2005).
[21] S. Wethekam and H. Winter, Phys. Rev. Lett. **96**, 207601 (2006).
[22] S. Wethekam and H. Winter, Nucl. Instrum. Methods Phys. Res. B **258**, 7 (2007).
[23] N. Bajales, J. Ferrón, and E. C. Goldberg, Phys. Rev. B **76**, 245431 (2007).
[24] W. Sesselmann, B. Woratschek, J. Küppers, G. Ertl, and H. Haberland, Phys. Rev. B **35**, 1547 (1987).
[25] H. Winter, J. Phys.: Condens. Matter **8**, 10149 (1996).
[26] S. A. Deutscher, X. Yang, and J. Burgdörfer, Phys. Rev. A **55**, 466 (1997).
[27] G. E. Makhmetov, A. G. Borisov, D. Teillet-Billy, and J. P. Gauyacq, Europhys. Lett. **27**, 247 (1994).
[28] K. Niedfeldt, E. A. Carter, and P. Nordlander, J. Chem. Phys. **121**, 3751 (2004).
[29] S. Wethekam, A. Mertens, and H. Winter, Phys. Rev. Lett. **90**, 037602 (2003).
[30] R. C. Monreal, L. Guillemot, and V. A. Esaulov, J. Phys.: Condens. Matter **15**, 1165 (2003).
[31] S. Wethekam, A. Mertens, and H. Winter, Nucl. Instrum. Methods Phys. Res. B **212**, 308 (2003).
[32] Yu. Bandurin, V. A. Esaulov, L. Guillemot, and R. C. Monreal, Phys. Rev. Lett. **92**, 017601 (2004).
[33] K. Kimura, T. Tsujioka, S. Tanaka, A. Nakamoto, K. Nakajima, and M. Suzuki, Phys. Rev. A **70**, 022901 (2004).
[34] Diego Valdés, J. M. Blanco, V. A. Esaulov, and R. C. Monreal, Phys. Rev. B **75**, 165404 (2007).
[35] D. Primetzhofer, S. N. Markin, J. I. Juaristi, E. Taglauer, and P. Bauer, Phys. Rev. Lett. **100**, 213201 (2008).
[36] H. H. Brongersma, M. Draxler, M. de Ridder, and P. Bauer, Surf. Sci. Rep. **62**, 63 (2007).
[37] N. V. Smith, C. T. Chen, and M. Weinert, Phys. Rev. B **40**, 7565 (1989).
[38] A. Kiejna, Phys. Rev. B **47**, 7361 (1993).
[39] A. Sarasola, V. M. Silkin, and A. Arnau, Phys. Rev. B **75**, 045104 (2007).
[40] M. Alducin, R. Diéz Muiño, and J. I. Juaristi, Phys. Rev. A **70**, 012901 (2004).
[41] S. Wethekam, Diego Valdés, R. C. Monreal, and H. Winter, Phys. Rev. B **78**, 033105 (2008).
[42] H. Hansen, A. Redinger, S. Messlinger, G. Stoian, Y. Rosandi, H. M. Urbassek, U. Linke, and T. Michely, Phys. Rev. B **73**, 235414 (2006).
[43] D. Gemmell, Rev. Mod. Phys. **46**, 129 (1974).
[44] R. Zimny and Z. L. Misković, Nucl. Instrum. Methods Phys. Res. B **58**, 387 (1991).
[45] R. Souda and M. Aono, Nucl. Instrum. Methods Phys. Res. B **15**, 114 (1986).
[46] Based on the classical image potential, this correction of the ion fractions may not be correct because incident ions and neutrals will follow different trajectories. However, this is not consistent with the present understanding for the difference of the interaction potentials for He^0 atoms and He^+ ions (closely related to the ground-state energy shift, see Sections II C and III B). For incident ions, this leads to an increase in the impact energy due to an image chargelike attraction of about 2 eV only. As the ion fractions for scattering of He^0 atoms do not show a pronounced dependence on the incident normal energy and the surviving ion fractions obtained for different beam energies coincide, we consider our correction as reasonable. Nevertheless, a restriction to the two lowest energies where reionization is negligible would not change our conclusions.
[47] W. H. Press, S. A. Teukolsky, W. T. Vetterling, and B. P. Flannery, *Numerical Recipes in* C^{++} (Cambridge University Press, Cambridge, England, 2002).
[48] D. P. Jackson, Surf. Sci. **43**, 431 (1974).
[49] S. Wethekam and H. Winter, Nucl. Instrum. Methods Phys. Res. B **258**, 48 (2007).
[50] D. J. O'Connor and J. P. Biersack, Nucl. Instrum. Methods Phys. Res. B **15**, 14 (1986).
[51] A. Schüller, G. Adamov, S. Wethekam, K. Maass, A. Mertens, and H. Winter, Phys. Rev. A **69**, 050901(R) (2004).
[52] S. Wethekam, A. Schüller, and H. Winter (unpublished).
[53] M. J. Puska and R. M. Nieminen, Phys. Rev. B **43**, 12221 (1991).
[54] N. Jean, M. I. Trioni, G. P. Brivio, and V. Bortolani, Phys. Rev. Lett. **92**, 013201 (2004).
[55] S. A. Cruz, E. Ley-Koo, and R. Cabrera-Trujillo, in *Computation in Modern Science and Engineering*, edited by T. E. Simons and G. Maroulis (Springer, New York, 2008), Vol. 963/2.
[56] L. A. Salmi, Phys. Rev. B **46**, 4180 (1992).
[57] R. Pfandzelter, Phys. Rev. B **57**, 15496 (1998).
[58] Diego Valdés, J. M. Blanco, V. A. Esaulov, and R. C. Monreal, Phys. Rev. Lett. **97**, 047601 (2006).
[59] In this work, the projectiles are scattered along high-indexed azimuthal directions of the surface plane (random orientation). One could wonder whether some important aspects are missing by not measuring along low-indexed directions. We think this is not the case. A similar theory as presented here for Al was used by some of the present authors in an analysis of experimental ion fractions for He^+ scattered from Ag(111) and Ag(110) surfaces both at random and low-indexed azimuthal directions in Refs. 34 and 58, obtaining good agreement between theory and experiment. It was found that differences between azimuthal directions are mainly a result of different interaction times and distances of closest approach whereas the physics involved is the same. Nevertheless, for a more detailed analysis of the lateral dependence of Auger neutralization rates and ground-state energy shifts, data for scattering along low-indexed directions would be needed.